

## Article

# Enhancing the Efficiency of Bi-Facial Photovoltaic Panels: An Integration Approach

Emad Abdelsalam <sup>1</sup>, Hamza Alnawafah <sup>2</sup>, Fares Almomani <sup>3,\*</sup>, Aya Mousa <sup>1</sup> and Hasan Qandil <sup>4</sup>

<sup>1</sup> Electrical and Energy Engineering Department, Al Hussein Technical University, Amman 11831, Jordan; emad.abdelsalam@htu.edu.jo (E.A.); aya.mousa@htu.edu.jo (A.M.)

<sup>2</sup> Mechanical Engineering Department, University of Wisconsin-Milwaukee, Milwaukee, WI 53211, USA; alnawaf2@uwm.edu

<sup>3</sup> Chemical Engineering Department, Qatar University, Doha P.O. Box 2713, Qatar

<sup>4</sup> Department of Mechanical Engineering, University of North Texas, Denton, TX 76207, USA; hassan.qandil@unt.edu

\* Correspondence: falmomani@qu.edu.qa

**Abstract:** This work presents a novel approach to increasing the efficiency of photovoltaic (PV) panels by integrating them with a cooling tower (CT). An infusion of water cools the hot, dry ambient air at the top of the CT. Due to gravity, the cooled air drops toward the base of the CT, where it interacts with a turbine placed at the bottom of the CT to produce electricity. The air then exits the CT base, creating a cooled air jet stream. The PV panels were placed at the base of the CT, right at the stream's exit. As the cooled air passes underneath the PV panels, it exchanges energy with the PV, reducing the panels' temperature. The results showed that the maximum annual efficiency improvement (6.831%) was observed using two rows of PV panels. The efficiency declined incrementally from 6.831% to 4.652% when the number of rows of PV panels was increased from two to twelve. The results also showed a significant improvement in the temperature of the PV panels. The best results were obtained at noon (maximum ambient temperature), where the solar panel temperature was lowered to 25 °C from 55 °C. Furthermore, the annual electrical energy generated with two rows of panels was 39,207.4 kWh without the CT, compared to 41,768.2 kWh with the CT. In addition, the results showed that with a 10 m diameter and 200 m height CT, the maximum number of PV rows that can be effectively cooled is 24. Future work will investigate integrating additional techniques to improve the system's efficiency further.

**Keywords:** photovoltaic cooling; cooling tower; efficiency; downdraft system; passive cooling



check for updates

**Citation:** Abdelsalam, E.; Alnawafah, H.; Almomani, F.; Mousa, A.; Qandil, H. Enhancing the Efficiency of Bi-Facial Photovoltaic Panels: An Integration Approach. *Sustainability* **2023**, *15*, 14786. <https://doi.org/10.3390/su152014786>

Academic Editors: Pietro Bartocci, Gloria Pignatta, Adel Juaidi and Amir Vadiie

Received: 18 August 2023

Revised: 28 September 2023

Accepted: 7 October 2023

Published: 12 October 2023



**Copyright:** © 2023 by the authors. Licensee MDPI, Basel, Switzerland. This article is an open access article distributed under the terms and conditions of the Creative Commons Attribution (CC BY) license (<https://creativecommons.org/licenses/by/4.0/>).

## 1. Introduction

Humans' improved living standards, industrial expansion, and rising global population counts have led to an ongoing demand for energy [1–4]. This growth has also led to a significant demand growth for finite fossil fuel sources to meet the daily life needs of citizens. Yet, this raises concerns about the long-term durability of these sources and their influence on the environment and society [5]. Furthermore, mindless energy consumption contributes to an environmental crisis with many consequences that affect the planet's well-being. The situation escalates when the rising demand for clean, fresh water is combined with the current and future rise in power usage [6–9] in generating clean forms of energy while reducing greenhouse gases (GHG) released because of using traditional energy sources [2,10]. However, relying on renewable energy sources remains commercially challenging due to production and manufacturing costs and, in some cases, the installed capacity costs. Many of the above reasons have prompted the world to concentrate on a technologically viable method of producing low-cost power using solar energy [11–13]. The primary focus of this research is solar energy integration with new technologies, as it is extensively utilized as a renewable energy source for energy generation and thermal

systems. Even though solar energy is viewed as a clean energy source, a wide range of chemicals are used in producing solar energy, such as photovoltaic panels, which adds to the overall cost and can have a substantial environmental impact [14]. As a result, modern technologies that use fewer chemicals, are easy to use and need minimal maintenance are required to minimize the impact of climate change [15,16]. Due to the ongoing production and installation of solar photovoltaic (PV) panels, the efficiency of this technology has significantly increased. Although 40% efficiency has been reported for laboratory testing conditions, economic and commercial panel efficiencies have proven to be substantially lower [17]. For example, monocrystalline PV cells can achieve a laboratory efficiency of around 24%, yet the practical efficiency is limited to 11–17% [17,18]. Temperature fluctuations also impact solar cells. Temperature variations affect the output power of the PV cells. Temperature significantly affects voltage, and as the temperature rises, the voltage decreases [19,20]. Furthermore, the impact of cooling conditions on PV panels' efficiency enhancement [19] has been tested. Since test results indicate that solar PV performance increases by 47% when cooled, a cooling system is proposed as a potential configuration for a residential solar PV design. PV panels were integrated around the circumference of the solar chimney power plant (SCPP) to be used as a heat sink to boost the plant's performance [21]. A proposal to submerge the PV panels in a water pool at the base of the SCPP to improve efficiency was presented [22]. Suggestions to integrate cooling tower technology with the SCPP to boost the performance of the SCPP have been addressed [23]. This study explores the potential of bi-facial photovoltaic (PV) panels, which stand out from their conventional monofacial counterparts. Unlike traditional panels that solely harness sunlight from the front, bi-facial PVs are adept at absorbing sunlight from both their front and back surfaces. This dual-sided absorption means they capture direct solar radiation and benefit from light reflected from adjacent environments. Such a unique design opens up pathways for substantial performance enhancements. Prior research, such as [24], provides empirical evidence of this augmented efficiency across varied terrains. Similarly, Ref. [25] brings to light the paramount importance of deploying optimal installation techniques to realize the full potential of these panels. Ref. [25] further elucidates the pivotal role of ground surface albedo in influencing the outcomes of bi-facial PVs. Interestingly, despite these panels' evident promise, few research endeavors have extensively delved into their application. This is particularly surprising given their transformative capabilities in the renewable energy landscape. Our investigation is motivated by this very gap. Not only do we aim to provide deeper insights into bi-facial PV technology, but we also endeavor to underscore why they should feature more prominently in academic and industrial research.

The novelty of this work is centered on using passive cooling from a renewable energy source (CT) to improve the efficiency of bi-facial PV panels. Specifically, the PV panels were placed at the base of the CT, right at the exit of the cool stream. As the cooled air passes underneath the PV panels, it exchanges energy with the PV, reducing the panels' temperature, hence improving the efficiency of the PV panels. The work structure starts with system integration, as described in Section 2. A mathematical model of the proposed integration is then presented. In the Section 3, a review of the weather data is presented, along with the performance of the CT and the effect of different parameters on the integration. The Section 3 particularly highlights the impact on the efficiency of the PV panels. Section 4 are presented at the end.

## 2. Materials and Methods

### 2.1. Proposed Integration

Figure 1a illustrates the structure of a CT integrated with the bi-facial PV panels. The design comprises a CT, a turbine, water sprinklers, and PV panels. The turbine is located at the base of the CT, while the sprinklers are located at the top. The PV panels are located outside the CT's base, surrounding the base's circumference. The physical dimensions of the different components of the stem are also shown in the figure. Figure 1b shows a comprehensive view of the proposed system from different angles. Figure 1b also shows

the arrangement of the PV panels based on the actual dimensions of the panels, arranged row-by-row around the circumference of the CT's base. The radius of one row is the length of the PV panel.

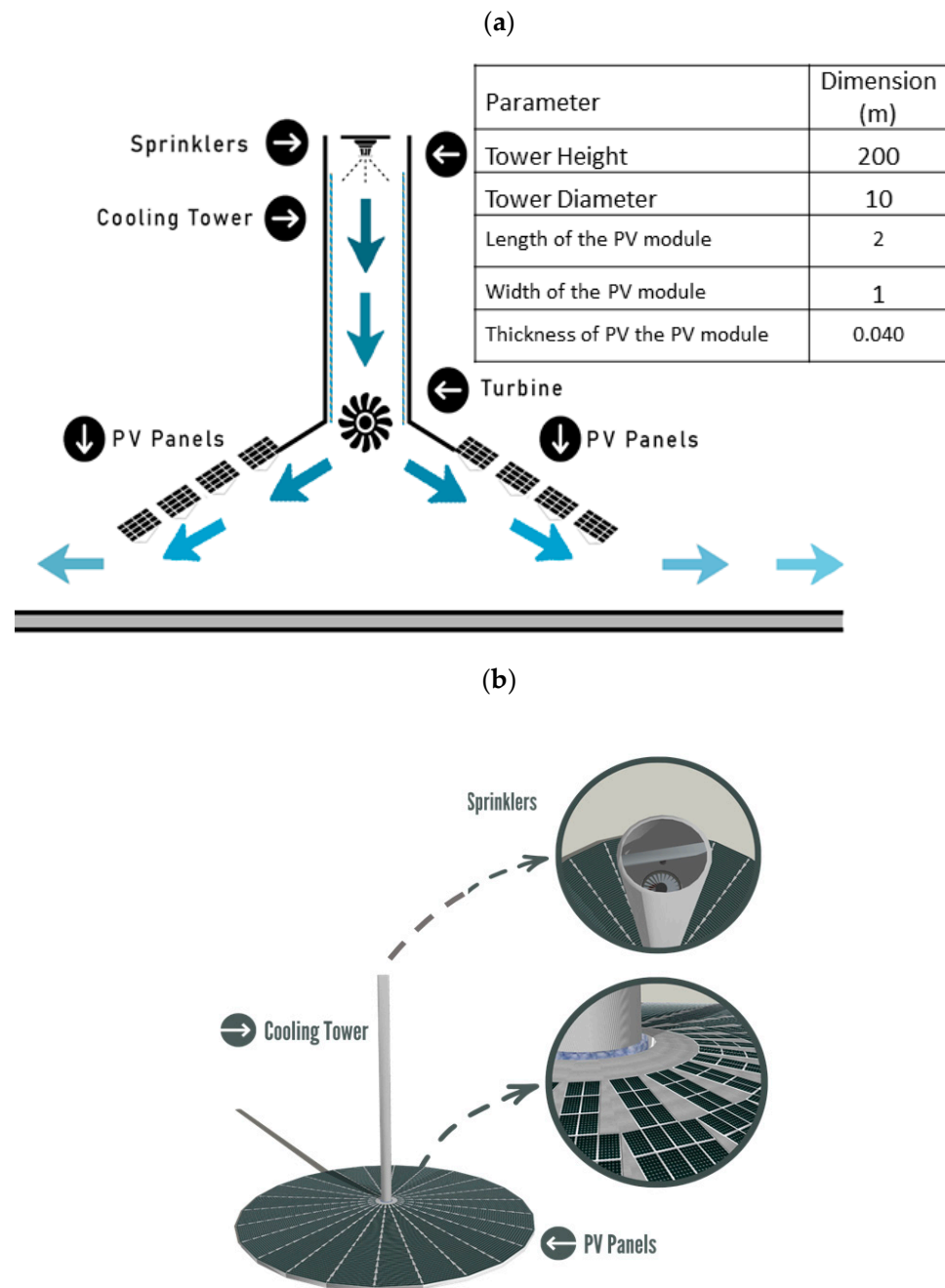


**Figure 1.** Illustration of the proposed system integration: (a) details of the cooling tower and PV panels are shown, and (b) PV panels surrounding the cooling tower.

The CT works by sprinkling water from the top, which contains the hot, dry surrounding air. The air becomes colder and heavier because of it absorbing the moisture from the mist. Gravity causes the air to fall toward the CT's base. A turbine at the base of the CT uses the streaming air to produce power. As the cooled air exits the base of the CT, it cools the surrounding PV panels. The impact of cooling the PV panels was studied in terms of efficiency and generated power.

## 2.2. Mathematical Model

A mathematical model was developed to ensure that the air and energy balance equations were maintained throughout the system, accounting for the impact on each segment of the bi-facial PV panels. Equations (1)–(10) were derived from the model to demonstrate how the bi-facial PV panels can be integrated with the CT. To enable numerical simulation and equation solving, the model was coded in MATLAB. The code processed weather data and computed the results hourly.

### 2.2.1. Bi-Facial Panels Segment

The model initiates the calculation of the bi-facial PV panels' temperature by determining the bi-facial irradiance received by the panels.

The bi-facial irradiance was determined using Equation (1), as follows (Gostein et al., n.d.) [26]:

$$G_{bifacial} = G \times (1 + alb) \quad (1)$$

where  $alb$  is the albedo value,  $G_{bifacial}$  is the bi-facial irradiance ( $W/m^2$ ), and  $G$  is total irradiance ( $W/m^2$ ).

Following the calculation of the bi-facial irradiance received by the panels, the model utilizes Equation (2) to determine the temperature of the PV panels. (Gostein et al., n.d.) [26]:

$$T_{pv} = T_a + \frac{G_{bifacial}}{(U_0 + U_1 \times Vw)} \quad (2)$$

The  $U_0$  and  $U_1$  values represent the PV panels' thermal transmittance and thermal conductance, respectively. These values are used in determining the overall thermal performance of the PV panels; based on the bi-facial PV panel data sheet, the values are:  $U_0 = 21.777 W/m^2 \cdot K$ ,  $U_1 = 9.855 W/m^2 \cdot K$ .

\*  $T_a$  is the ambient temperature, and  $Vw$  is the wind speed

\* It is important to note that when the CT is not functioning or the system is operating solely in PV mode, the ambient temperature ( $T_a$ ) serves as the baseline temperature. Conversely, during the operation of the CT, the cooled air temperature ( $T_{vout}$ ), indicated in Equation (8), is utilized as the reference temperature for calculations. The same principle applies to the wind speed variable ( $Vw$ ).

The temperature profile of the air below the PV panels was established through the resolution of Equation (3) [24], as represented below:

$$\alpha_c * G * (1 - \eta_c) = Am * [\tau_t \alpha_t G (1 - \beta) + \sigma * \left( \frac{(T_{pv} + T_t) * (T_{pv}^2 + T_t^2)}{(\frac{1}{ec}) + (\frac{1}{et}) - 1} \right) * (T_{pv} - T_t) - ((5.7 + 3.8 * Vw) * (T_t - T_a)) - (T_t - T_a)] \quad (3)$$

where:

$\alpha_c * G * (1 - \eta_c)$  is the temperature gradient of the air under the PV panels,  $A_m$  is the PV panel area,  $T_t$  is the temperature of the air under the PV panels,  $\beta$  is the packing factor ( $0.0045/^\circ C$ ),  $\alpha_t$  is the absorptivity of the bi-facial PV panels (0.8),  $\tau_t$  is the transmissivity of the bi-facial PV panels (0.012),  $ec$  is the emissivity of the bi-facial cell (0.99),  $\alpha_c$  is the absorptivity of the bi-facial cell (0.85),  $\eta_c$  is the efficiency of the bi-facial cell (0.22), and  $et$  is the emissivity of the bi-facial PV panels glass (0.90).

The efficiency  $\eta$  ( $T_{pv}$ ) of bi-facial solar panels in the field was determined using Equation (4).

$$\eta(T_{pv}) = \eta(STC) * \{1 + \beta * (T_{pv} - 298K)\} \quad (4)$$

Here,  $\beta$  denotes the temperature coefficient, which has a value of  $-0.280/^\circ C$ . The bi-facial solar panel's efficiency is represented by  $\eta$  ( $STC$ ), with  $STC$  Signifying Standard Test Condition.

### 2.2.2. Cooling Tower Section

The enthalpy of the vapor at the top of the CT was determined using the following calculation:

$$i_{vap} = i_{air} + \omega_{vap} i_{wtr} \quad (5)$$

$$i_{air} = c_{p,air} T_o \quad (6)$$

Similarly, the enthalpy value of the water was ascertained as follows:

$$i_{wtr} = c_{p,wtr} T_{wtr} \quad (7)$$

The vapor temperature was calculated as below:

$$c_{p,air} T_o + (\omega_{air} 2501.3 + T_o 1.86) = c_{p,air} T_{vap} + (\omega_{vap} 2501.3 + T_{vap} 1.86) \quad (8)$$

where 2501.3 kJ/kg is the specific enthalpy of water vapor at 0 °C, and 1.86 kJ/kg °C, is the specific heat of water vapor at constant pressure.

The velocity of the air exiting at the CT was determined utilizing the following equation [22]:

$$V_{ch} = \sqrt{2gH_{ch} \frac{T_{ch,ext} - T_{out}}{T_{out}}} \quad (9)$$

The electrical output power generated from the CT was determined using the following equation:

$$P_{elc} = \frac{1}{2} \rho_{en,ch} C_f A_{ch} V_{ch}^3 \quad (10)$$

where  $C_f$  is the turbine efficiency, 0.42.

### 2.2.3. Model Validation

In [27], the authors installed temperature sensors on bi-facial PV panels in a field test and collected ambient temperature, wind speed, and solar irradiance data. They used the data to run a temperature calculation model and compared the results to the measured temperatures of the PV panels. In this study, we integrated the SolarTech XF123 bi-facial solar panel into a solar chimney solar power plant (SCPP) design, capitalizing on its unique attribute: pronounced transparency. Traditional PV panels predominantly absorb and convert solar radiation with limited transparency. However, the bi-facial SolarTech XF123 model facilitates a significant amount of sunlight to penetrate, making it an ideal candidate for solar chimney applications. While capturing solar radiation from both sides for electricity generation, its transparency simultaneously enhances the greenhouse effect in the solar chimney's collector area, boosting its thermal efficiency. The electrical specifications of this panel include an Open Circuit Voltage (Voc) of 68.2 V, a Short Circuit Current (Isc) of 10.4 A, a Maximum Power Point Voltage (Vmpp) of 58.7 V, and a Maximum Power Point Current (Imp) of 9.8 A, delivering a peak power (Pmax) of 390 W. The study found that the model predictions agreed with the PV panels' measured temperatures, with a mean absolute error of less than 1 degree Celsius. The study also found that the model was able to accurately predict the effect of wind speed on the temperature of the PV panels. The study also performed a sensitivity analysis, where it was found that the model's results were most sensitive to the value of the U1 parameter, which represents the thermal conductance of the PV panel. The difference between the PV module temperature and the ambient temperature was validated against the results reported by [26], as shown in Table 1. The results show a close correlation between the baseline measurements and our results.

**Table 1.** Validation results of the bi-facial PV temperature with the results in [26].

Solar Irradiance (W/m <sup>2</sup> )	T <sub>mod</sub> -T <sub>amb</sub> (°C) (Baseline [26])	T <sub>mod</sub> -T <sub>amb</sub> (°C) (This Work)	Percent Error (%)
200	5	4.82	3.6
400	10	9.64	3.6
600	15	14.46	3.6
800	20	19.28	3.6
1000	24	24.1	−0.42

The RSM error and R<sup>2</sup> of the results were found to be 0.443 and 0.998, respectively, showing a close correlation between the model and predicted values. The percent error was continuously below 5% for all predicted values.

### 3. Results and Discussion

This section begins with analyses of the weathering profile, as weather conditions significantly affect the efficiency of a CT and solar PV. An investigation of the CT's electricity production performance is presented while varying the humidity and ambient temperature values. This helps understand the impact of cool air output from a CT on PV energy production. The succeeding section addresses some thermal characteristics of the PV panels, significantly, how the cool air speed and temperature from a CT will alter its performance. Afterward, the standalone PV power output is investigated versus PV panels with an integrated CT. Finally, it highlights the efficiency enhancement of solar PV panels.

#### 3.1. Weather Profile

Year-round weather data were collected for Doha, Qatar (25°17'9.9816" N and 51°32'5.3412" E), the study locale. The data were acquired at an hourly rate for the temperature, humidity, wind speed, and solar irradiance. Figure 2 shows the weather data profile on 21 June. The data from this day were used in all corresponding 24 h figures in the subsequent sections. The profile indicates that solar irradiance begins at 05:00 with 54 W/m<sup>2</sup> until 17:00 with 118 W/m<sup>2</sup>. The peak solar irradiance for the day was at noon, with an intensity of 845 W/m<sup>2</sup>. Furthermore, temperatures during the daytime ranged from 28.0 °C to 38 °C. However, at night, the range in temperature was observed to be between 30.2 °C and 34.4 °C. The profile of Figure 2 for onsite wind shows a minimum speed of 2.1 m/s and a maximum of 4.6 m/s. Wind speed values directly contribute to the cooling of the PV panels and, thus, the production of electrical power. In addition, relative humidity plays a significant role in the performance of a CT. As also shown in the profile, relative humidity measurements varied from 19% to 84% in the daytime, with 24% to 83% at night.

#### 3.2. Performance for CT

The hourly electricity production from the CT, cross-examined with respective humidity and temperature profiles, is illustrated in Figure 3. As seen in the figure, the humidity is relatively high (~80%) from midnight till around 6:00 in the morning. It then declines to about 20% at about 15:00, to climb again and reach 60% late at night. The humidity showed a giant swing over the 24 h. Contrary to that, the temperature profile fluctuates, but not as much as the humidity. It starts at 30 °C at midnight and gradually increases to reach 40 °C at noon, and is almost steady until 15:00. Then it starts to decline to reach 30 °C again late at night. The solid black line represents the electrical power produced by the CT. The CT is OFF from midnight until 7:00 in the morning. It is ON for the rest of the day with fluctuating power production.

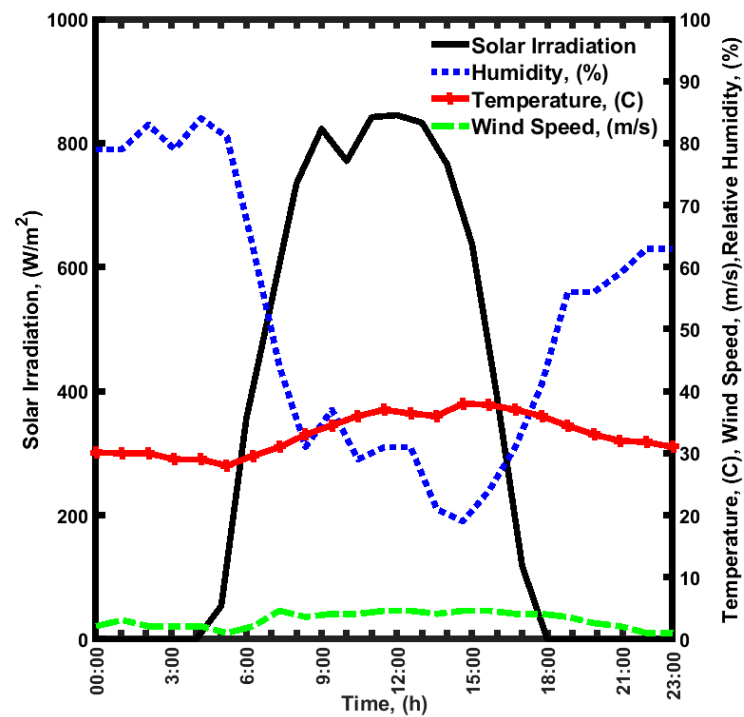


Figure 2. Profiles of hourly weather data, measured on 21 June.

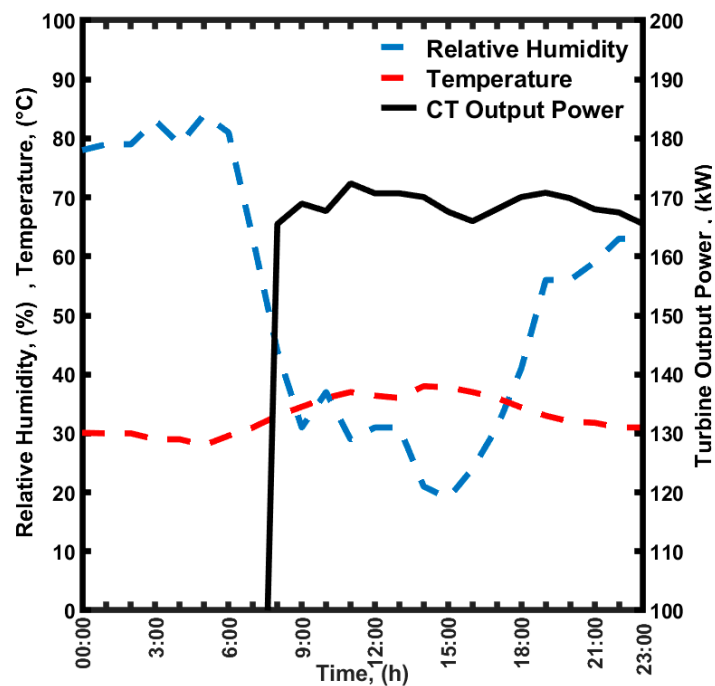


Figure 3. Hourly electricity production from the CT was cross-examined with respective humidity and temperature profiles on 21 June.

The CT's performance is enhanced with higher ambient temperatures and lower humidity levels. The ambient temperature must be higher than the water temperature to cool the hot ambient air. Hence, the higher the contrast between the ambient temperature and the water spray, the cooler the end temperature of the vapor produced. Per Equation (9), the air velocity increases with the increased difference between the ambient and vapor

temperatures. Consequently, per Equation (10), the electrical power produced is enhanced with higher speeds.

In contrast, as the humidity rises, the electrical power produced falls. That is because, at high humidity, more electrical energy will be consumed, pumping additional water for an elevated humidity of the already humid air. Consequently, the net energy produced is insignificant or diminished. Hence, the dryer the air is, the lower the amount of water sprayed, and therefore, the lower the electrical power consumed. The essential CT product is the volume and temperature of exiting cooled air, as it is a critical factor in cooling the solar panels. This is discussed in the next section.

### 3.3. PV Performance Examination, Standalone and with CT

#### 3.3.1. CT-Cooled Air Effect on the Solar Panels' Temperature

Displayed in Figure 4 are the single-row solar panel temperature profiles for both the standalone configuration (no CT, black solid line) and the integrated configuration (with CT, red dashed line). Data are shown from midnight until morning and from sunset until midnight, and the temperature profiles are identical since the PV panel is not operating during these times due to the absence of solar irradiance. Figure 4 reveals how the PV panels' temperatures without a CT climb early in the morning to peak at 55 °C around noon. They then declines to reach an ambient temperature (30 °C) around sunset. This is a typical temperature response of the panels, which increases with higher ambient temperatures and irradiance values. However, the CT-integrated PV panels' temperatures are much lower. Figure 4 depicts that the CT's cooling effect on PV panels is down in the early hours because of the slight difference between the sprayed water temperature (from the nozzles) and the ambient temperature. However, as the ambient temperature continues to climb above the sprayed water temperature, as seen in Figure 3, the CT produces cooler air. Hence, the best results were obtained at noon (maximum ambient temperature), where the solar panel temperature was lowered to 25 °C from 55 °C. A significant 5 °C to 30 °C change in panel temperature was noticeable between the two configurations (with and without CT). Hence, the PV panels were effectively cooled by the CT.

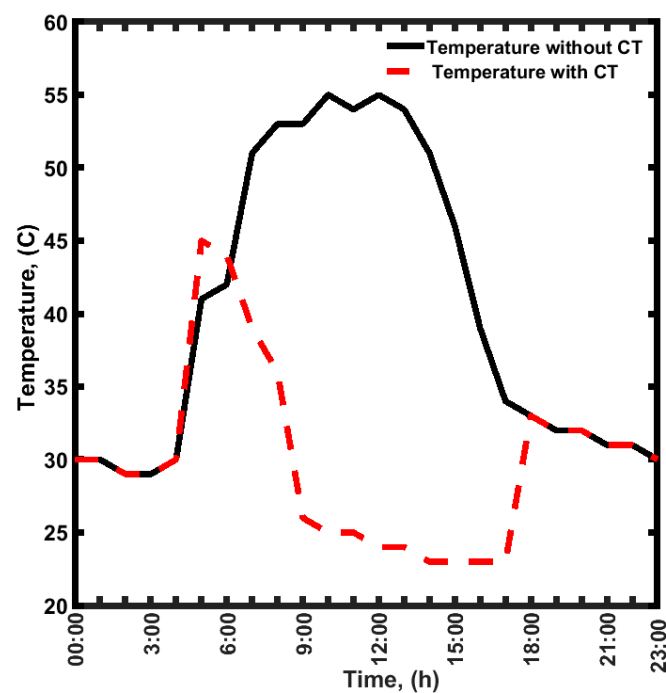


**Figure 4.** Temperature profiles of the PV panels for both the standalone configuration (no CT) and the integrated configuration (with CT).

The previous section showed that the CT improved the cooler air and effectively reduced the temperature of the PV panels. This was due to the temperature and velocity of the cool air. Figure 5 shows the subpanel air velocities. The solid black line corresponds to the wind velocity when the PV panels are in a standalone configuration. The wind profile is the same as shown in Figure 2. The wind velocity shows a normal fluctuation during the 24 h, ranging from 2 m/s to about 5 m/s. The corresponding ambient temperature is anywhere between 30 °C and 40 °C, as shown in Figure 2. These temperatures and velocities are not sufficient to cool the panels.

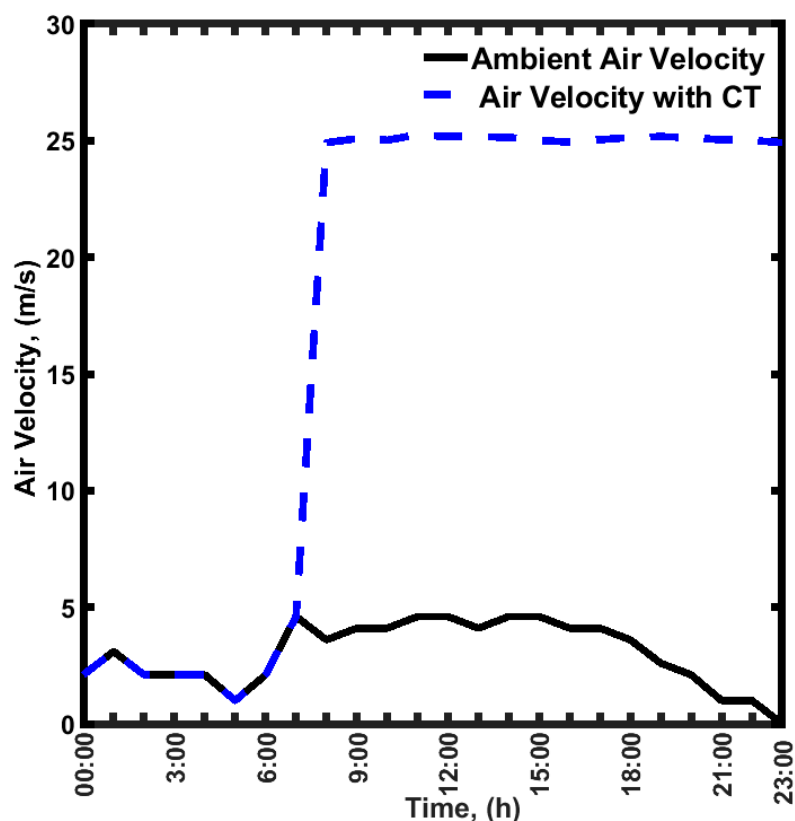


**Figure 5.** Subpanel wind velocity profiles for the standalone configuration (no CT) and the integrated configuration (with CT).

In contrast, the CT-produced cooled air velocity (dashed blue line) almost flatlines at 25 m/s. The figure displays identical speeds for the ambient and CT-cooled air from midnight until around 7:00 in the morning. This is because the CT was OFF during this time, as shown in Figure 2, then further explained in Section 3.2. However, from 7:00 until midnight, the CT constantly produced cool air. The high velocity of the CT air, combined with its low temperature, effectively cooled down the PV panels. Hence leading to improved power production, which is discussed next.

Figure 6 illustrates the single-row PV power productions (blue dashed line without CT, red dotted–solid line with CT) with correspondence to irradiance (black solid line). The single row is formed of individual panels located adjacent to each other and around the circumference of the CT. The electricity production started with small productions in the early hours of the day to peak at noon with 12.9 kW for the no CT configuration. Both productions slow down after 15:00 and cease around 18:00. Noticeably, the CT-integrated power production improves and shifts more than that of no CT. Minimal improvement was observed between 6:00 and 8:00, which can be attributed to lower solar irradiance.

Furthermore, as is shown in Figure 2, the CT was OFF until almost 7:00, and as is shown in Figure 3, the ambient and CT-cooled temperatures were the same. Hence, the

power production enhancement is insignificant. However, the significant improvement in power production of the PV panels reached its maximum at peaked irradiance (noon time), as the CT integration improved the power production from 12.9 kW to 14.77 kW. This can result from the panel temperature dropping due to cooling, as explained in Figure 4.

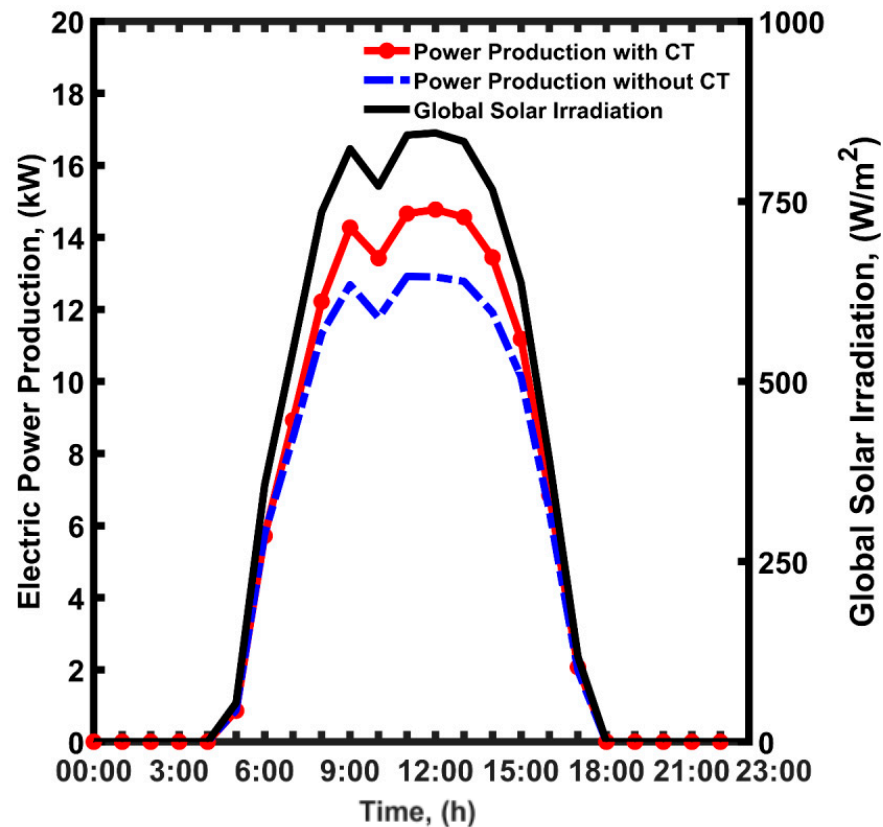


Figure 6. The power production of the bi-facial PV panels for a complete day on 21 June.

The results showed that the CT turns ON around 7:00, which produces cool air. The air exits the CT to travel underneath the surrounding PV panels. The air travels around 25 m/s per Figure 5. The air exchanges energy with the panels, which results in cooling it. The correlation between the CT ON mode and the reduction in the PV panels' temperature is evident in Figure 4. This led to higher electrical productivity, as seen in Figure 6. Contrary to that, when the CT was OFF, the temperature and PV power production results for both configurations were identical without improvement. Hence, the PV power production improvement was due to an improvement in their efficiency, which is discussed next.

### 3.3.2. PV Efficiency Improvement

Figure 7 shows the monthly average PV efficiencies (blue solid line without CT, red solid line with CT) over one year, calculated based on Equation (4).

Efficiency calculations were performed for the case of one row of PV panels. The cases of more panels are discussed in the next section. The results show that the PV efficiency with no CT begins with modest values in January and peaks later in May. It declines again to fair values in December. This is somewhat expected based on the weather conditions year-round in Doha. Although the trend of PV efficiency with an integrated CT follows a similar pattern, it has shifted quite a bit. The results show that from December through January, the efficiency of the PV panels was not improved; this is likely due to the ambient air temperature not exceeding the sub-thirties. This can also be attributed to the CT not operating during this time (winter) due to high humidity. However, the PV efficiency continued to improve throughout the year and reached a maximum in June/July.

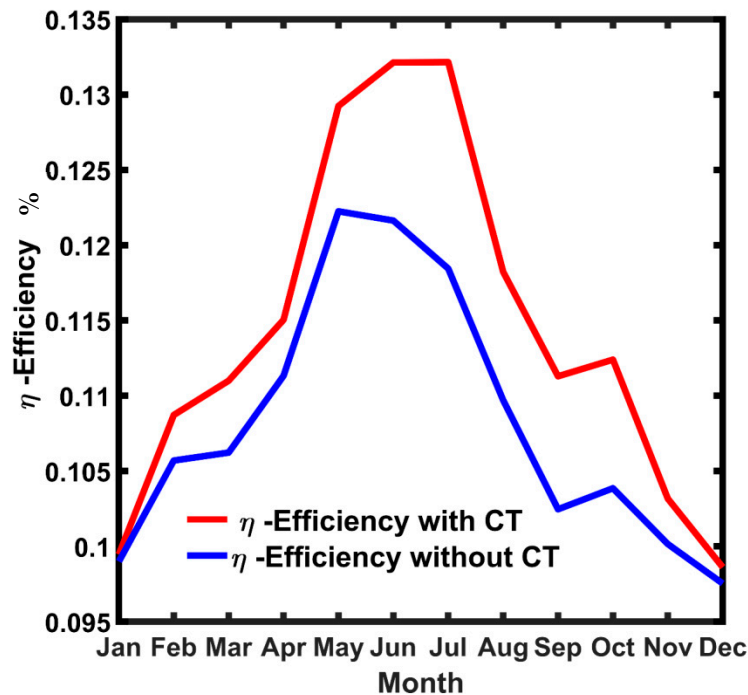


Figure 7. Average monthly efficiency trends of the PV panels for both configurations.

### 3.3.3. Efficiency Enhancement for the Larger Number of Panels

This study was extended to assess the efficiency improvement for many PV panels. The number of rows of PV panels was extended from two rows to 12, with two row increments, then a big jump to 24, and then to 34 rows. The results show that the maximum efficiency improvement was observed in two rows, as shown in Figure 8. The efficiency declined incrementally from 6.831% to 4.652% between rows two to twelve. The next step was to double the number of rows (24). The efficiency calculated was 4.493. However, at 34 rows, the efficiency improvement dropped to 0.129, indicating no further improvement can be achieved beyond the 34 rows. The results are meaningful because it is expected that the exiting air velocity from the CT will decline as you move away from the base of the CT.

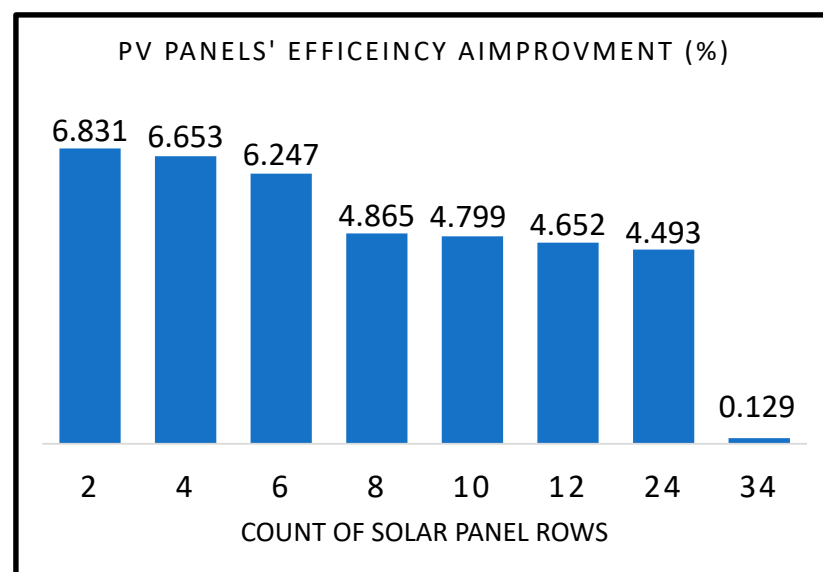


Figure 8. Mean annual PV efficiency enhancements vs. the number of panel rows.

Furthermore, it is also expected that this air temperature will rise as it exchanges energy with the PV panels. Hence, given the dimensions and specifications of the CT, 24 is the recommended number of PV panels to maintain minimum efficiency improvement at 4.5%. Although the results suggest that the integration is scalable, the proposed system has inherent limitations, which are discussed next.

The results show that the PV efficiency increased by about 6.8% with the CT's integration. Comparing our work to what is available in the literature, previous research looked at improving efficiency for a single PV panel. However, this study looks at a cooling technique for the entire PV power plant. Hence, our efficiency improvement represents the overall efficiency of all of the PV panels. Table 2 summarizes some prior studies of PV panel cooling and its corresponding PV efficiency enhancements [28].

**Table 2.** Prior studies of PV panel cooling techniques.

Authors	PV Panel Type	Cooling Methods	Efficiency Improvement
[29]	Polycrystalline	Water sprayed (active cooling)	Efficiency increased up to 20%
[30]	Monocrystalline	Airflow streamed over the backside of the solar panels	Efficiency increased up to 2.4%
[31]	Monocrystalline	Water circulated (active cooling)	Efficiency increased up to 12.5%
[32]	Polycrystalline	Water absorber plate with PV/T system	Efficiency increased up to 10.4%
[33]	Monocrystalline	Ducts cooled by air conditioners	Efficiency increased up to 7.2%

#### 4. Conclusions

A novel approach to integrating bi-facial PV panels with a cooling tower was presented. The study demonstrated the feasibility of integrating bi-facial PV panels with cooling towers to improve the panels' efficiency. The results showed an impressive efficiency improvement when integrating the PV panels with the CT, compared with a baseline case of standalone PV panels. Based on the given dimensions of the CT, it is recommended to integrate up to 24 PV rows to achieve a reasonable ~5% annual efficiency improvement. The cooling tower could, on its own, operate to produce electricity 24/7 depending on the weather conditions. The PV panels work during the daytime only due to the need for solar radiation to produce electricity. It was demonstrated that the jet-cooled air from the cooling tower cools off the PV panels, improving their efficiency. The weather conditions play a vital role in achieving the desired results. The cooling tower performs best in dry, hot weather. The dryer the air, the cooler the jet air, hence, better cooling for the PV panels. Accordingly, the deployment location for the combined system becomes very critical. It is recommended to deploy the proposed approach in remote areas where access to electricity is limited or does not exist.

Furthermore, it is recommended to ensure access to nearby seawater or other water sources. Future work will address some of the system's limitations, such as scalability issues. Furthermore, future work might focus on further assessing the feasibility of integrating other technologies to improve the system's performance.

**Author Contributions:** Conceptualization, F.A.; Methodology, E.A. and A.M.; Software, E.A. and H.A.; Validation, E.A. and F.A.; Investigation, H.A. and A.M.; Resources, F.A.; Data curation, H.A. and H.Q.; Writing—original draft, F.A. and H.Q. All authors have read and agreed to the published version of the manuscript.

**Funding:** This research received no external funding.

**Institutional Review Board Statement:** Not applicable.

**Informed Consent Statement:** Not applicable.

**Data Availability Statement:** The data presented in this study is contained within the article.

**Conflicts of Interest:** The authors declare no conflict of interest.

## References

1. Mohsin, M.; Abbas, Q.; Zhang, J.; Ikram, M.; Iqbal, N. Integrated effect of energy consumption, economic development, and population growth on CO<sub>2</sub> based environmental degradation: A case of transport sector. *Environ. Sci. Pollut. Res.* **2019**, *26*, 32824–32835. [[CrossRef](#)]
2. Kannan, N.; Vakeesan, D. Solar energy for future world—A review. *Renew. Sustain. Energy Rev.* **2016**, *62*, 1092–1105. [[CrossRef](#)]
3. Al-Othman, A.; Darwish, N.N.; Qasim, M.; Tawalbeh, M.; Darwish, N.A.; Hilal, N. Nuclear desalination: A state-of-the-art review. *Desalination* **2019**, *457*, 39–61. [[CrossRef](#)]
4. Salameh, T.; Ghenai, C.; Merabet, A.; Alkasrawi, M. Techno-economical optimization of an integrated standalone hybrid solar PV tracking and diesel generator power system in Khorfakkan, United Arab Emirates. *Energy* **2020**, *190*, 116475. [[CrossRef](#)]
5. Al Ketife, A.M.D.; Almomani, F.; EL-Naas, M.; Judd, S. A technoeconomic assessment of microalgal culture technology implementation for combined wastewater treatment and CO<sub>2</sub> mitigation in the Arabian Gulf. *Process Saf. Environ. Prot.* **2019**, *127*, 90–102. [[CrossRef](#)]
6. Takalkar, G.; Bhosale, R.; Kumar, A.; Almomani, F.; Khraisheh, M.; Shakoob, R.; Gupta, R. Transition metal doped ceria for solar thermochemical fuel production. *Sol. Energy* **2018**, *172*, 204–211. [[CrossRef](#)]
7. Franzluebbers, A.J. Cattle grazing effects on the environment: Greenhouse gas emissions and carbon footprint. In *Management Strategies for Sustainable Cattle Production in Southern Pastures*; Elsevier: Amsterdam, The Netherlands, 2020; pp. 11–34.
8. Alami, A.H.; Abu Hawili, A.; Tawalbeh, M.; Hasan, R.; Al Mahmoud, L.; Chibib, S.; Mahmood, A.; Aokal, K.; Rattanapanya, P. Materials and logistics for carbon dioxide capture, storage and utilization. *Sci. Total Environ.* **2020**, *717*, 137221. [[CrossRef](#)] [[PubMed](#)]
9. Almomani, F.; Judd, S.; Bhosale, R.R.; Shurair, M.; Aljaml, K.; Khraisheh, M. Intergraded wastewater treatment and carbon bio-fixation from flue gases using *Spirulina platensis* and mixed algal culture. *Process Saf. Environ. Prot.* **2019**, *124*, 240–250. [[CrossRef](#)]
10. Infield, D.; Freris, L. *Renewable Energy in Power Systems*; John Wiley & Sons: Hoboken, NJ, USA, 2020.
11. Zhou, X.; Wang, F.; Ochieng, R.M. A review of solar chimney power technology. *Renew. Sustain. Energy Rev.* **2010**, *14*, 2315–2338. [[CrossRef](#)]
12. Dhahri, A.; Omri, A. A review of solar chimney power generation technology. *Int. J. Eng. Adv. Technol.* **2013**, *2*, 1–17.
13. Kasaeian, A.; Ghalamchi, M.; Ahmadi, M.H.; Ghalamchi, M. GMDH algorithm for modeling the outlet temperatures of a solar chimney based on the ambient temperature. *Mech. Ind.* **2017**, *18*, 216. [[CrossRef](#)]
14. Tawalbeh, M.; Al-Othman, A.; Kafiah, F.; Abdelsalam, E.; Almomani, F.; Alkasrawi, M. Environmental impacts of solar photovoltaic systems: A critical review of recent progress and future outlook. *Sci. Total Environ.* **2021**, *759*, 143528. [[CrossRef](#)]
15. Rosa, L.; Chiarelli, D.D.; Rulli, M.C.; Dell'Angelo, J.; D'Odorico, P. Global agricultural economic water scarcity. *Sci. Adv.* **2020**, *6*, eaaz6031. [[CrossRef](#)]
16. Jia, X.; Klemeš, J.J.; Alwi, S.R.W.; Varbanov, P.S. Regional Water Resources Assessment using Water Scarcity Pinch Analysis. *Resour. Conserv. Recycl.* **2020**, *157*, 104749. [[CrossRef](#)]
17. Wong, J.; Sridharan, R.; Shanmugam, V. Quantifying edge and peripheral recombination losses in industrial silicon solar cells. *IEEE Trans. Electron Devices* **2015**, *62*, 3750–3755. [[CrossRef](#)]
18. Gaglia, A.G.; Lykoudis, S.; Argiriou, A.A.; Balaras, C.A.; Dialynas, E. Energy efficiency of PV panels under real outdoor conditions—An experimental assessment in Athens, Greece. *Renew. Energy* **2017**, *101*, 236–243. [[CrossRef](#)]
19. Dubey, S.; Sarvaiya, J.N.; Seshadri, B. Temperature dependent photovoltaic (PV) efficiency and its effect on PV production in the world—A review. *Energy Procedia* **2013**, *33*, 311–321. [[CrossRef](#)]
20. Slimani, M.E.A.; Amirat, M.; Kurucz, I.; Bahria, S.; Hamidat, A.; Chaouch, W.B. A detailed thermal-electrical model of three photovoltaic/thermal (PV/T) hybrid air collectors and photovoltaic (PV) module: Comparative study under Algiers climatic conditions. *Energy Convers. Manag.* **2017**, *133*, 458–476. [[CrossRef](#)]
21. Alkasrawi, M.; Abdelsalam, E.; Alnawafah, H.; Almomani, F.; Tawalbeh, M.; Mousa, A. Integration of Solar Chimney Power Plant with Photovoltaic for Co-Cooling, Power Production, and Water Desalination. *Processes* **2021**, *9*, 2155. [[CrossRef](#)]
22. Kiwan, S.; Al-Nimr, M.; Salim, I. A hybrid solar chimney/photovoltaic thermal system for direct electric power production and water distillation. *Sustain. Energy Technol. Assess.* **2020**, *38*, 100680. [[CrossRef](#)]
23. Abdelsalam, E.; Almomani, F.; Kafiah, F.; Almaitta, E.; Tawalbeh, M.; Khasawneh, A.; Habash, D.; Omar, A.; Alkasrawi, M. A New Sustainable and Novel Hybrid Solar Chimney Power Plant Design for Power Generation and Seawater Desalination. *Sustainability* **2021**, *13*, 12100. [[CrossRef](#)]
24. Abdelsalam, E.; Alnawafah, H.; Almomani, F.; Mousa, A.; Jamjoum, M.; Alkasrawi, M. Efficiency Improvement of Photovoltaic Panels: A Novel Integration Approach with Cooling Tower. *Energies* **2023**, *16*, 1070. [[CrossRef](#)]
25. Liang, T.S.; Praveetoni, M.; Deline, C.; Stein, J.S.; Kopecek, R.; Singh, J.P.; Luo, W.; Wang, Y.; Aberle, A.G.; Khoo, Y.S. A review of crystalline silicon bifacial photovoltaic performance characterization and simulation. *Energy Environ. Sci.* **2019**, *12*, 116–148. [[CrossRef](#)]

26. Gostein, M.; Pelaez, S.A.; Deline, C.; Habte, A.; Hansen, C.W.; Marion, B.; Newmiller, J.; Sengupta, M.; Stein, J.S.; Suez, I. Measuring Irradiance for Bifacial PV Systems: Preprint. Available online: <https://www.nrel.gov/docs/fy21osti/80281.pdf> (accessed on 17 August 2023).
27. Riedel-Lyngskær, N.; Berrian, D.; Mira, D.A.; Protti, A.A.; Poulsen, P.B.; Libal, J.; Vedde, J. Validation of bifacial photovoltaic simulation software against monitoring data from large-scale single-axis trackers and fixed tilt systems in Denmark. *Appl. Sci.* **2020**, *10*, 8487. [[CrossRef](#)]
28. Parthiban, R.; Ponnambalam, P. An Enhancement of the Solar Panel Efficiency: A Comprehensive Review. *Front. Energy Res.* **2022**, *10*, 1090. [[CrossRef](#)]
29. Benato, A.; Stoppato, A.; De Vanna, F.; Schiro, F. Spraying Cooling System for PV Modules: Experimental Measurements for Temperature Trends Assessment and System Design Feasibility. *Designs* **2021**, *5*, 25. [[CrossRef](#)]
30. Besheer, A.H.; Smyth, M.; Zacharopoulos, A.; Mondol, J.; Pugsley, A. Review on recent approaches for hybrid PV/T solar technology. *Int. J. Energy Res.* **2016**, *40*, 2038–2053. [[CrossRef](#)]
31. Tan, W.C.; Saw, L.H.; Thiam, H.S.; Yusof, F.; Wang, C.-T.; Yew, M.C. Investigation of water cooled aluminium foam heat sink for concentrated photovoltaic solar cell. *IOP Conf. Ser. Earth Environ. Sci.* **2019**, *268*, 012007. [[CrossRef](#)]
32. Al-Waeli, A.H.; Sopian, K.; Kazem, H.A.; Chaichan, M.T. Photovoltaic Solar Thermal (PV/T) Collectors Past, Present and Future: A Review. *Int. J. Appl. Eng. Res.* **2016**, *11*, 10757–10765. Available online: <http://www.ripublication.com> (accessed on 14 December 2022).
33. Elminshawy, N.A.S.; El-Ghandour, M.; Elhenawy, Y.; Bassyouni, M.; El-Damhogi, D.G.; Addas, M.F. Experimental investigation of a V-trough PV concentrator integrated with a buried water heat exchanger cooling system. *Sol. Energy* **2019**, *193*, 706–714. [[CrossRef](#)]

**Disclaimer/Publisher’s Note:** The statements, opinions and data contained in all publications are solely those of the individual author(s) and contributor(s) and not of MDPI and/or the editor(s). MDPI and/or the editor(s) disclaim responsibility for any injury to people or property resulting from any ideas, methods, instructions or products referred to in the content.